Materials Research Letters

ISSN: 2166-3831 (Online) Journal homepage: www.tandfonline.com/journals/tmrl20

Ultra-high-strain-rate deformation induced HCP-to-FCC phase transformation and its interaction with {112} twin in pure Ti

Qian Liu, Bohao Zhou, Xing Zhang, Yuqian Wang, Wanting Sun, Qifei Zhang, Yafei Wang, Gaofei Liang, Hao Wang, Shuangjie Chu & Bo Mao

To cite this article: Qian Liu, Bohao Zhou, Xing Zhang, Yuqian Wang, Wanting Sun, Qifei Zhang, Yafei Wang, Gaofei Liang, Hao Wang, Shuangjie Chu & Bo Mao (2026) Ultra-high-strain-rate deformation induced HCP-to-FCC phase transformation and its interaction with {112} twin in pure Ti, Materials Research Letters, 14:1, 38-47, DOI: 10.1080/21663831.2025.2584206

To link to this article: https://doi.org/10.1080/21663831.2025.2584206

MATER. RES. LETT.
2026, VOL. 14, NO. 1, 38–47
https://doi.org/10.1080/21663831.2025.2584206

MATERIALS RESEARCH LETTERS
Taylor & Francis
Taylor & Francis Group

REPORT

Ultra-high-strain-rate deformation induced HCP-to-FCC phase transformation and its interaction with {11$\bar{2}$2} twin in pure Ti

Qian Liu[a], Bohao Zhou[a], Xing Zhang[b], Yuqian Wang[c], Wanting Sun[d], Qifei Zhang[a,e], Yafei Wang[a], Gaofei Liang[e], Hao Wang[f], Shuangjie Chu[a] and Bo Mao[a]

[a]School of Materials Science and Engineering, Shanghai Jiao Tong University, Shanghai, People's Republic of China; [b]School of Mechanical and Electric Engineering, Soochow University, Suzhou, People's Republic of China; [c]Department of Mechanical Engineering, University of Nevada-Reno, Reno, USA; [d]School of Engineering, Lancaster University, Lancaster, UK; [e]Baowu Special Metallurgy Co., Ltd., Shanghai, People's Republic of China; [f]Shanghai Engineering Research Center of Laser Intelligent Manufacturing, Shanghai Institute of Laser Technology Co., Ltd., Shanghai, People's Republic of China

ABSTRACT

In this work, HCP-to-FCC phase transformation and its interaction with {11$\bar{2}$2} compression twins (CTWs) in CP-Ti under ultra-high-strain-rate compression ($\sim 10^6$/s) was investigated. Muti-scale characterization and analysis demonstrate the both B- and P-type FCC_{Ti} lamellae are profusely generated and exhibit significant growth capability and intensive interaction with the CTWs. Particularly, two adjacent FCC_{Ti} lamellae with a twinning relationship can be formed within the CTW and matrix, respectively. Moreover, two adjacent FCC_{Ti} lamellae with nearly identical orientation can be formed within the two different CTW variants. Two possible mechanisms were proposed to account for this unique phenomenon.

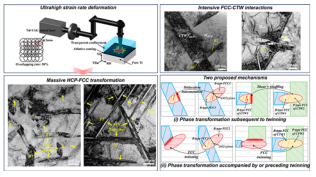

ARTICLE HISTORY
Received 7 July 2025

KEYWORDS
CP-Ti; ultra-high-strain-rate deformation; HCP-to-FCC phase transformation; phase interface; dislocation activity

1. Introduction

Dislocation slip and deformation twining are two major mechanisms governing the plastic deformation for titanium (Ti) and its alloys with a hexagonal close-packed (HCP) structure. In addition to these typically deformation modes, deformation-induced HCP-to-FCC phase transformation has been identified in commercially pure Ti (CP-Ti), offering a complementary mode to accommodate the plastic strain [1]. Based on the crystallographic orientation relationship (OR) between the HCP and FCC phase, two distinct ORs have been well documented: (i) B-type OR characterized by $\{0001\}_{HCP}//\{111\}_{FCC}$ and $<\bar{2}110>_{HCP}//<110>_{FCC}$ can be accomplished via the gliding of 30° Shockley partial dislocations on every two (0001) basal planes [2,3]. (ii) P-type OR defined by $\{10\bar{1}0\}_{HCP}//\{110\}_{FCC}$ and $<0001>_{HCP}//<001>_{FCC}$ can be achieved via shear-shuffle mechanism through successive gliding of two-layer disconnections or pure-shuffle mechanism through collective gliding of a four-layer disconnection on $\{10\bar{1}0\}$prismatic plane [4]. The presence of FCC phase not only accommodates the plastic deformation but also enhances the ductility, which is attributed to their abundant slip systems and effective strain partition capability, leading to the uniform plastic flow [5,6].

Due to its scientific significance and potential practical applications, extensive studies through both experimental and numerical analysis have been carried out to elaborate the formation mechanism [7], interfacial structure [8], grain size-dependence [9] of HCP-to-FCC phase

CONTACT Bo Mao bmao@sjtu.edu.cn School of Materials Science and Engineering, Shanghai Jiao Tong University, Shanghai 200240, People's Republic of China

Supplemental data for this article can be accessed online at https://doi.org/10.1080/21663831.2025.2584206.

transformation in CP-Ti and its effect on the subsequent plastic deformation behavior [10] under a variety of deformation conditions, such as room temperature compression [11], cryogenic compression [2], cold rolling [4], shot peening [12], and high-pressure torsion [13]. Nevertheless , limited attention has been paid to investigate the HCP-to-FCC phase transformation behavior in CP-Ti under ultra-high-strain-rate (UHSR) deformation (10^6/s), despite numerous studies showed a prominent strain-rate dependency of stress-induced phase transformation in Ti and other metallic alloys [14–17]. Our recent studies have demonstrated that HCP metals exhibited unique twinning modes and dislocation behavior during UHSR deformation [18–20]. Meanwhile, given the prevalent activation of deformation twinning in Ti alloys, it is expected that HCP-to-FCC phase transformation and deformation twins could be concurrently activated and interact with each other, but the interplay between these two mechanisms remains rarely studied and insufficiently understood. Addressing this research gap is essential for advancing the development of UHSR-based processing of Ti and its alloys.

In this work, the deformation-induced HCP-to-FCC phase transformation and its interaction with $\{11\bar{2}2\}$ deformation twins in a CP-Ti under UHSR compression ($\sim 10^6$/s) was systematically investigated using multi-scale microstructure characterizations. The UHSR compression was realized by laser shock peening (LSP) , which is recognized as a laser-based surface processing technique that utilizes high-energy laser pulses to generate intense shock wave for the enhancement in mechanical performance of Ti alloys [19]. By producing exceptionally high triaxial stresses and distinctive shock-wave propagation dynamics, LSP provides a unique means to reveal the UHSR shock response of metallic materials [21–25]. It can be found that both B- and P-type FCC_{Ti} are profusely generated after UHSR deformation. The FCC_{Ti} lamellae are not only observed within the α-Ti matrix but also within the $\{11\bar{2}2\}$ compression twin (CTW) regions. The interaction between FCC_{Ti} lamellae and CTW results in unique microstructural features and has never been reported before. It is expected that these findings in this study can provide in-depth insights into the deformation-induced HCP-to-FCC phase transformation mechanism in Ti alloys and inspire further exploration of its interactions with deformation twinning.

2. Materials and methods

In this work, CP-Ti samples were provided by Baowu special metallurgy Co., Ltd.. Chemical composition, detailed sample preparation procedures, and the initial microstructure of the as-received material can be referred to Supplementary Note 1. Based on the inverse pole figure (IPF) map and transmission electron microscopy (TEM) images (Fig. S1), the twins and FCC phases cannot be detected within the initial microstructure. To investigate the UHSR deformation behavior of CP-Ti, LSP processing was carried out with a Nd:YAG pulsed laser system. Experimental setup and detailed mechanism of the UHSR deformation is illustrated in Supplementary Note 2. Subsequently, multi-scale microstructure characterizations were performed on the LSP-treated sample, including optical microscopy (OM), electron backscatter diffraction (EBSD), transmission Kikuchi diffraction (TKD), TEM and high-resolution TEM (HR-TEM), and the detailed characterization procedures are illustrated in Fig. S3.

3. Results and discussion

Figure 1 shows the surface microstructure of the LSP-treated CP-Ti. A distinct circle surrounded by lenticular twins is observed (Figure 1(a)). EBSD analysis (Figure 1(b–f)) reveals that these twins can be identified as $\{11\bar{2}2\}$ CTWs, $\{10\bar{1}2\}$ tension twins (TTWs) and $\{11\bar{2}1\}$ TTWs, according to the well-defined rotation angle/axis relationships of different twinning modes [26]. However, some specific regions comprising fine lamellar structures (marked by the yellow arrows in Figure 1(d2 and f2)) cannot be well-resolved on the basis of EBSD analysis. To further reveal these microstructural features, cross-sectional TKD EBSD analysis was performed on a lamella extracted from the center of the LSP-processed area (Figure 1(g–i)). It demonstrates the formation of numerous FCC_{Ti} lamellae with an average thickness of 94.5 nm (marked by red color in the phase map in Figure 1(g)). By measuring the OR relationship between the FCC and HCP phases, both B- and P-type FCC phase are activated, with multiple variants labeled as B1-B3 and P1-P4, respectively. The detailed procedures for determining the OR and variant types relative to their HCP parent grains can be referred to Supplementary Note 4 (Fig. S4 and Table S4). The frequency of B and P-type FCC formed within the HCP matrix are summarized in Fig. S5. It should be noted that the FCC lamellae are not only formed within the HCP matrix but also within the CTW1 and CTW2 variants, suggesting the significant growth capability of FCC phases under UHSR deformation. It must be emphasized that some researchers proposed that the FCC phases in Ti originate from hydride or oxide during sample preparation [27,28]. To rule out this possibility, electron energy loss spectroscopy (EELS) analysis was performed on the samples processed by LSP

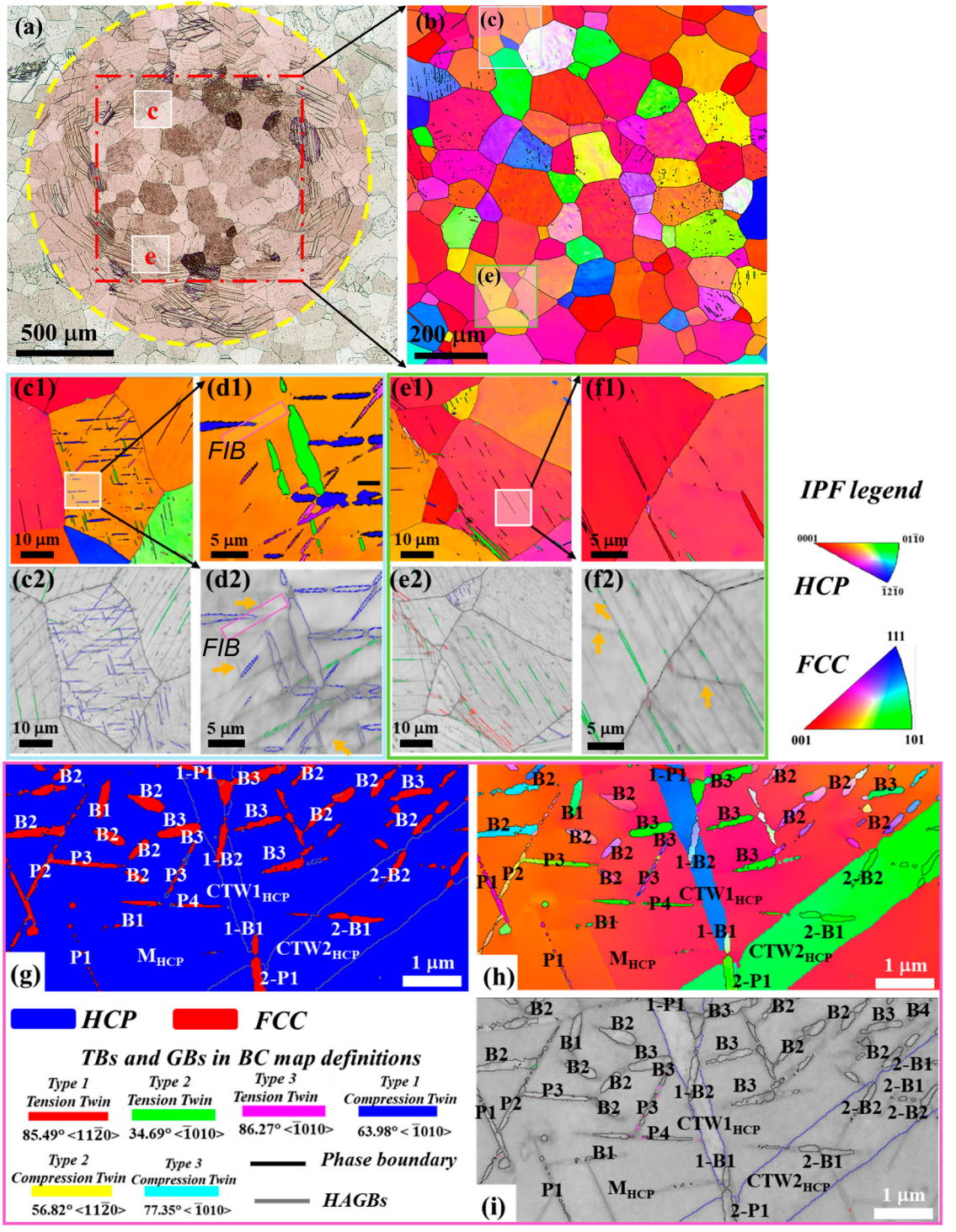

Figure 1. LSP-induced surface deformation analysis: (a) OM image. (b) IPF map of the squared region in (a). (c1-c2) and (e1-e2) are enlarged regions from (b). (d1) and (f1) show further magnified areas. (c2-d2) and (e2-f2): BC maps corresponding to (c1-d1) and (e1-f1), respectively, showing that some lenticular structures marked by yellow arrows cannot be determined. The sampling location for the TKD analysis was marked by the pink boxes in (d1, d2). The occurrence of HCP-to-FCC phase transformation in the CTWs: (g) Phase map, (h) IPF map, (i) BC map.

and the results are shown in Fig. S6. The EELS spectrum revealed that the FCC phases was neither hydride nor oxide, confirming their generation was resulted from UHSR deformation-induced phase transformation.

To reveal the microstructural and crystallographic features of the FCC lamellae, HR-TEM analysis was carried out on some specific areas and the results are shown in Figure 2. FCC_{Ti} nano-lamellas with

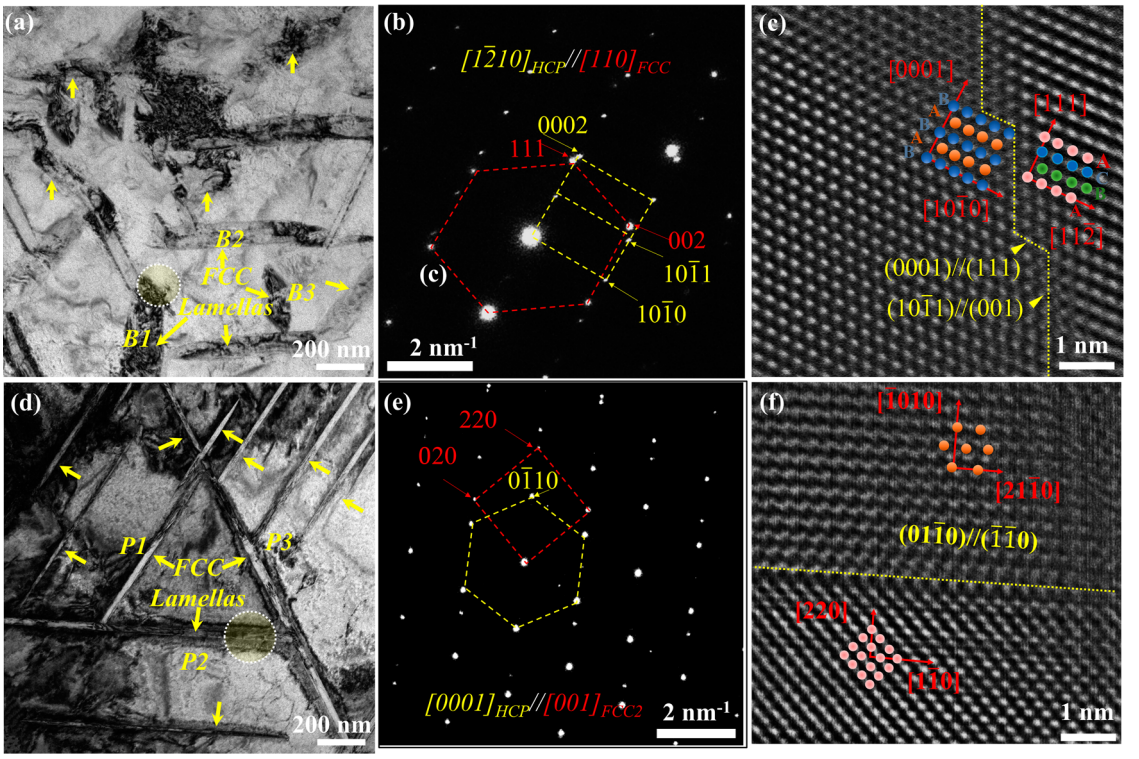

Figure 2. TEM images of the (a) B-type and (c) P-type FCC_{Ti} in LSP-treated CP-Ti. (b) and (e) are the SAED patterns that obtained from the white circle in (a) and (d), respectively. HR-TEM images showing (c) the stepped interfaces between B-type FCC_{Ti} and HCP matrix, and (f) a straight interface between P-type FCC_{Ti} and HCP matrix.

two distinct morphologies are observed within the HCP matrix, i.e. irregular (Figure 2(a)) and needle-like morphology (Figure 2(d)). The corresponding selected area electron diffraction (SAED) patterns of the circled areas as marked in Figure 2(a,d) present the OR between the FCC_{Ti} lamellae and the HCP matrix, as shown in Figure 2(b,e), respectively. For the irregular FCC_{Ti} lamellae (Figure 2(b)), the OR between the FCC_{Ti} lamellae and HCP matrix can be determined as $(0001)_{HCP}//(111)_{FCC}$ and $[1\bar{2}10]_{HCP}//[110]_{FCC}$. This crystallographic relationship can identify the irregular lamellae as B-type FCC_{Ti} variants (labeled as Bi , $i = 1, 2, 3$). In contrast, the needle-like FCC_{Ti} lamellae (Figure 2(e)) exhibit a different OR with $(01\bar{1}0)_{HCP}//(110)_{FCC}$ and $[0001]_{HCP}//[001]_{FCC}$, which corresponds to P-type FCC_{Ti} variant (labeled as Pi, $i = 1, 2, 3$). Figure 2(c,f) display the HR-TEM observation of the interfacial structure between FCC_{Ti} lamellae and the HCP matrix, respectively. As shown in Figure 2(c), the interface exhibits the faceted morphology consisting of short $(0001)_{HCP}//(111)_{FCC}$ and long $(10\bar{1}1)_{HCP}//(200)_{FCC}$ segments, which is different from the commonly observed phase boundaries consisting of the $(0001)_{HCP}//(111)_{FCC}$ interfaces. In contrast, the interface of P-type is exactly parallel to the $(01\bar{1}0)_{HCP}//(110)_{FCC}$ habit plane (Figure 2(f)), revealing the variant selection and interfacial structure of the HCP-to-FCC phase transformation in CP-Ti.

The discrepancy in terms of the morphology and interfacial characteristics of the B- and P-type FCC_{Ti} under UHSR deformation may be ascribed to their different formation mechanisms. As shown in Figure 2(c), the B-type FCC_{Ti} phase transformation can be accomplished via the gliding of Shockley partial dislocations on every two (0001) basal planes, resulting in the change in stacking sequence from … ABABAB … to … ABCABC … . Due to mutual repulsion between the Shockley partial dislocations, stepped interfaces can be observed [11]. Moreover, the UHSR deformation significantly deteriorates the cooperative lateral glide of the partial dislocations, thereby impeding the lateral growth and coalescence of the terraces to advance the phase boundary [29]. In contrast, the growth of the P-type FCC_{Ti} is governed by the successive gliding of two-layer steps on $(01\bar{1}0)$ prismatic plane induced by a shear-shuffle or pure shuffling mechanism [10]. Under UHSR deformation, the dislocation motion may be insufficient to accommodate the applied shock strain, atomic shuffling that directly advances the phase boundary appears to be more efficient and becomes the primary mechanism, resulting in the formation of straight interface and needle-like morphology of the FCC phases.

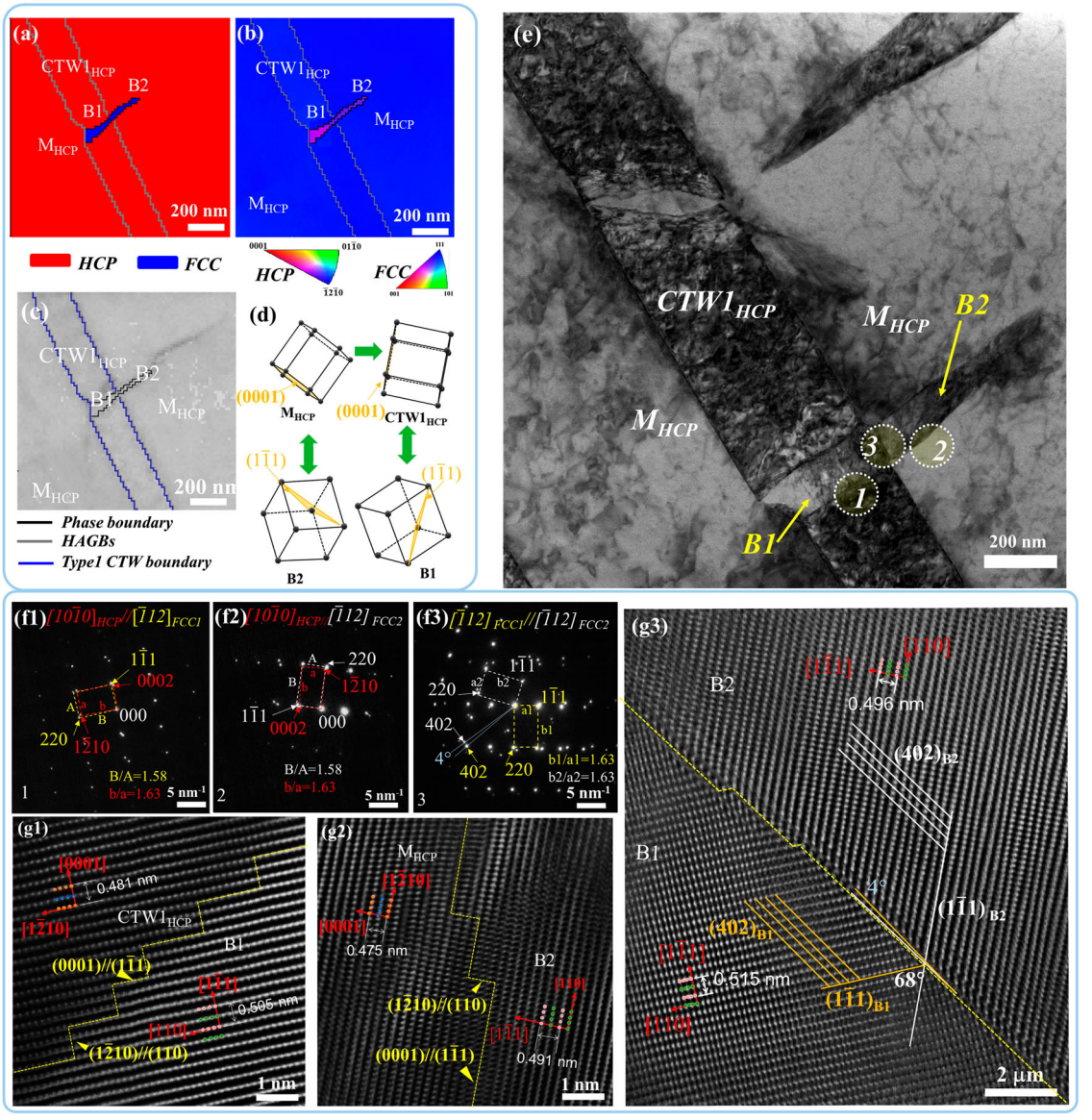

Figure 3. Microstructure analysis of the B-type FCC_{Ti} pair along the CTW boundary in LSP-treated CP-Ti: (a) Phase map, (b) IPF map, and (c) BC map. (d) Unit cells of different grains. (e) TEM image. (f1-f3) the SAED patterns and (g1-g3) HR-TEM images corresponding to regions 1, 2 and 3 in (e).

One prominent characteristic of the microstructure in CP-Ti after UHSR deformation is the intensive interaction between FCC_{Ti} and deformation twins. Figure 3(a–c) displays fine lenticular FCC_{Ti} (highlighted in blue in phase map) is formed within the HCP phase. As shown in Figure 3(b,c), a pair of adjacent FCC_{Ti} (B1 and B2) phase can be observed within the $\{11\bar{2}2\}$ twin (marked as $CTW1_{HCP}$) and the adjacent HCP matrix grains (M_{HCP}), respectively. Figure 3(d) illustrates the corresponding ORs between FCC and HCP grains. Figure 3(e) shows the TEM image of the interaction areas which are marked by the white circle 1-3 and will be characterized by the HR-TEM and SAED in detail. As shown in Figure 3(f1), when the electron beam is parallel to the $[10\bar{1}0]_{HCP}//[\bar{1}12]_{FCC1}$ of area 1, two sets of diffraction spots were observed, the B/A ratio within the yellow dashed box is 1.58, while the b/a ratio within the red dashed box is 1.63. This difference in ratios unequivocally confirms that one set of diffraction spots corresponds to the HCP structure, and the other set corresponds to the FCC structure. The SAED patterns form regions 1 and 2 in Figure 3(e) further confirm that these FCC_{Ti} variants are identified as B-type FCC_{Ti} structure (Figure 3(f1 and f2)), which is characterized by the OR of $(0001)_{HCP}//(1\bar{1}1)_{FCC}$ and $[10\bar{1}0]_{HCP}//[\bar{1}12]_{FCC}$. These are labeled by B1 (within $CTW1_{HCP}$) and B2 (within M_{HCP}), respectively. Furthermore, the SAED patterns of region 3 reveals a unique interface between B1 and

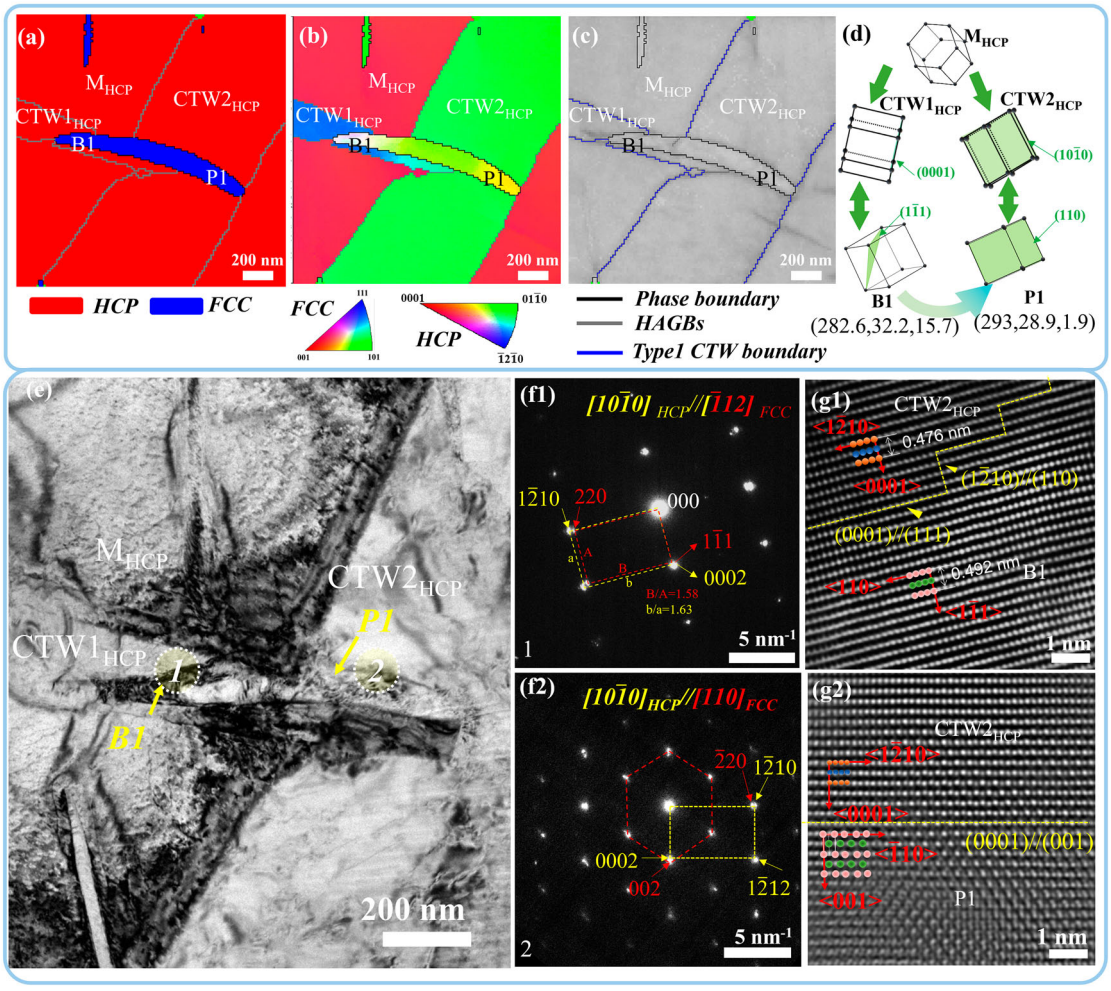

Figure 4. Microstructure analysis of B- and P-type FCC_{Ti} pair in adjacent CTW1 and CTW2 variants in LSP-treated CP-Ti: (a) Phase map, (b) IPF map, and (c) BC map, (d) Unit cells of different grains, (e) TEM image. (f1, f2) SAED patterns and (g1, g2) HR-TEM images corresponding to regions 1 and 2 in (e).

B2, which exhibits twin-like diffraction spots and a ~4° splitting angle of the (402) planes. The identification of HCP-FCC interface is challenging due to similar stacking sequences along the $[10\bar{1}0]_{HCP}//[\bar{1}12]_{FCC}$, but it is also should be noted that this HCP-to-FCC phase transformation is accompanied by volume expansion [12]. As depicted in Figure 3(g1 and g2), the interplanar distance of $(1\bar{1}1)$ plane in B1 and B2 is determined as 0.505 nm and 0.491 nm, respectively, while the (0001) planes in $CTW1_{HCP}$ and $CTW2_{HCP}$ are determined as 0.481 nm and 0.475 nm, respectively. These differences in lattice spacing and strain contrast enables the identification of phase boundaries (marked by yellow dotted lines) and the faceted interfaces along $(0001)_{HCP}//(1\bar{1}1)_{FCC}$ and $(1\bar{2}10)_{HCP}//(110)_{FCC}$. As shown in Figure 3(g3), the step-like twin boundary(TB) delineated by the yellow line was highlighted. By tracking the (402) planes of the B1 and B2, the 4° orientation misalignment between B1 and B2 can also be validated, corroborating the observed discrepancy in the (402) reflections. Similar occurrences of imperfect twin orientation relationships have also been observed in the$\{11\bar{2}\overset{N}{2}\}$ twinning mode [30,31] and $\{10\overset{N}{1}2\}$ twinning mode [32,33]. These phenomena are attributed to the accumulation of partial dislocations resulting from the interaction between the matrix dislocations and the twin boundary. At the B1/B2 interface, the misorientation angle between the $(1\overset{N}{1}1)$ planes of the B1 and B2 is 68°, close to the misorientation of $\{11\bar{2}2\}$ twin (63.98±5° along the $<10\bar{1}0>$). Moreover, the B1/B2 interface shares the common (402) planes (Figure 3(e3)), which is different from the formation of $\{111\}<112>$ twin within the FCC structure during HCP-to-FCC transformation [12,34,35].

Notably, a lenticular FCC_{Ti} lamella appears in the region where $CTW1_{HCP}$ and $CTW2_{HCP}$ interact (Figure 4(a)), occupying the space above both CTW1 and

$CTW2_{HCP}$. The IPF map (Figure 4(b)) shows a continuous orientation gradient in the FCC_{Ti} lamella, with no distinct high angle grain boundary (HAGBs), suggesting a gradual lattice rotation. By calculating the crystallographic relationship among the FCC_{Ti}, $CTW1_{HCP}$, and $CTW2_{HCP}$ (Table S1-S3), it is evident that FCC_{Ti} adopts a B-type OR with $CTW1_{HCP}$, referred to as B1. In contrast, when FCC_{Ti} is located within $CTW2_{HCP}$, it adopts a P-type OR with $CTW2_{HCP}$, denoted as P1. Figure 4(d) also shows the OR between M_{HCP}, $CTW1_{HCP}$, $CTW2_{HCP}$, B1, and P1. As presented in Figure 4(e), TEM observation confirms that the lamella constitutes a single FCC_{Ti} grain spanning two CTWs. To better examine the OR among $CTW1_{HCP}$, $CTW2_{HCP}$, and the FCC structures, SAED analysis on the regions outlined in white circles in Figure 4(e) was conducted. The OR between $CTW1_{HCP}$ and B1 is $[10\bar{1}0]_{HCP}//[\bar{1}12]_{FCC}$, $(0001)_{HCP}//(1\bar{1}1)_{FCC}$, $(1\bar{2}10)_{HCP}//(110)_{FCC}$ (Figure 4(f1)), while the OR between $CTW2_{HCP}$ and P1 is $[10\bar{1}0]_{HCP}//[110]_{FCC}$, $(0001)_{HCP}//(001)_{FCC}$, $(1\bar{2}10)_{HCP}//(\bar{1}10)_{FCC}$ (Figure 4(f2)). These results further reveals that the FCC_{Ti} within $CTW1_{HCP}$ and $CTW2_{HCP}$ exhibit different ORs: the B1 and $CTW1_{HCP}$ is identified as B-type OR, while the P1 and $CTW2_{HCP}$ is P-type OR. Figs. 4g1 and 4g2 show the HR-TEM images of the interfacial structure of B1/$CTW1_{HCP}$ and P1/$CTW2_{HCP}$, respectively. Similar to the analysis method in Figure 3(g1 and g2), the B1/$CTW1_{HCP}$ interface is discernible through {111} plane and {0002} plane spacings and strain contrast (Figure 4(g1)). The interface also displays stepped morphology, which is characterized by $(0001)_{HCP}//(111)_{FCC}$ and $(1\bar{2}10)_{HCP}//(110)_{FCC}$ (marked by yellow dotted line). Figure 4(g2) presents HRTEM image, captured along the $[10\bar{1}0]_{HCP}//[110]_{FCC}$, further confirming the common interface between the P1 and CTW2 is (0001)//(001).

Based on the above microstructure analysis, massive HCP-to-FCC phase transformation can be identified under UHSR deformation, showing significant growth capability and distinct interaction behavior with $\{11\bar{2}2\}$ TBs and CTW-CTW boundaries. Unlike the formation of micron-scale deformation twins and a few parallel FCC structures under low-strain-rate deformation [1,3,36,37], the microstructure evolution under UHSR deformation presents unique features. These features stem from the extremely short timescale ($\sim 10^6$ s^{-1}), the presence of high triaxial stresses, and the distinctive shock-wave propagation dynamics. One mechanism responsible for the unique feature is the phase 'transmission' or 'transmutation' activity induced by UHSR deformation. Previous works have demonstrated that deformation twins can 'transmit' or 'transmute' through adjacent grains under sufficiently high stress [38,39]. Accordingly, to maintain homogeneous deformation under UHSR, FCC_{Ti} could likewise propagate from one grain into its adjacent grains. However, the sequence of the HCP-to-FCC phase transformation and the occurrence of deformation twinning under UHSR deformation remains undetermined in the present study. Here we propose two possible mechanisms responsible for the unique microstructural features observed in Figures 3 and 4, as schematically illustrated in Figure 5. We named the first one as 'Phase transformation occurs subsequent to twinning' (Figure 5(a,b)), and the second 'Phase transformation occurs accompanied with or prior to twinning' (Figure 5(c,d)). The following sections discuss both scenarios in detail.

(i) Phase transformation subsequent to twinning

As shown in Figure 5(a,b), shear stress on the basal plane of CTW1 activates $1/3 < 10\bar{1}0 >$ Shockley partial dislocations, promoting FCC nucleation within CTW1. These partial dislocations continue slip and terminate at the $\{11\bar{2}2\}$ TB, causing localized stress that enables their transmission across the TB without generating a residual dislocation [40]. This dislocation transmission is facilitated by the favorable OR between the CTW and their matrix, which preserves the Burgers vector of partials dislocations and enabling their glide into the adjacent matrix grains [41]. The basal plane acts as the K2 plane of CTW, which aligns on either side of the common $(11\bar{2}2)$ plane. Consequently, the newly formed B-type FCC2 in the matrix grains exhibits a symmetric relationship with B-type FCC1 oriented along the (402) plane. Differently, when the FCC phase grows inside CTW1 and encounters a CTW-CTW boundary (Fig. 5b), dislocation transmission is hindered, leading to localized stress concentration. This localized stress promotes dislocation glide and drives a shear–shuffling transformation mechanism that converts $(01\bar{1}0)_{CTW1}$ plane into (111) plane of the FCC_{Ti} in CTW2. As a result, the B-type FCC_{Ti} continues to grow and traverses the CTW-CTW boundary. The newly formed FCC remains B-type with CTW1 but attains a P-type OR with CTW2. This observation is consistent with atomistic predictions that a double-layered $(01\bar{1}0)$ plane in the HCP grain can transform into the (111) plane in the FCC structure via shear and atomic shuffling [42].

(ii) Phase transformation accompanied by or preceding twinning

An alternative sequence in which the FCC-HCP transformation may occur first, followed by twinning in both the matrix and the FCC phase, ultimately forming CTW and the corresponding B1 or P1-type FCC phase may also

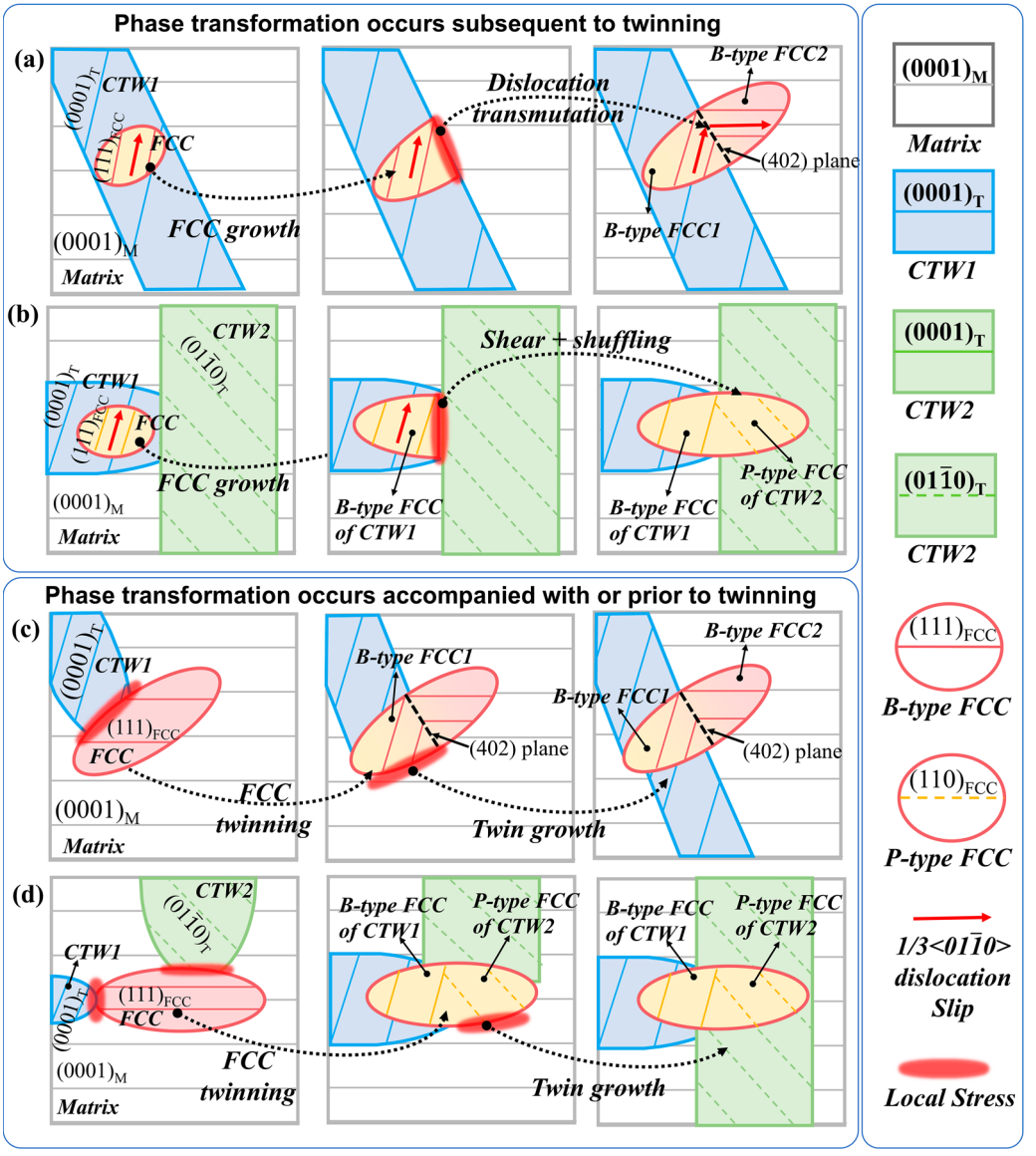

Figure 5. Proposed mechanisms of the HCP-to-FCC phase transformation and its interaction with {11$\bar{2}$2} twin in CP-Ti processed by LSP based on the two possible sequences: (a, b) HCP-FCC transformation occurs within the CTW followed by the deformation twinning. (c, d) HCP-FCC transformation occurs together with or before deformation twinning. Mechanism responsible for: (a, c) B-type FCC_{Ti} lying along the {11$\bar{2}$2} CTW boundary and forming a 'twin-like' structure, (b, d) B-type FCC_{Ti} and P-type FCC_{Ti} sharing the almost identical crystallographic features occurring within the CTW1 and CTW2, respectively.

be possible and schematically illustrated in Figure 5(c,d). The UHSR activates 1/3 < 10$\bar{1}$0 > partials on the basal plane in the matrix triggers HCP-to-FCC phase transformation, forming B-type FCC_{Ti}. In the meanwhile, CTW1 also formed and interacts with the FCC. The impingement of the CTW on the pre-existing FCC may generate interface stress concentrations that triggers deformation twinning in the FCC itself [38]. In the case of partial contact (Figure 5(c)), twinning occurs locally within the contact zone. The twinned FCC (B-type FCC1) retains a B-type OR with CTW1, while the untwinned part (B-type FCC2) retains its original lattice, establishing a twin relationship with FCC1. The lattice correspondence between FCC1 and FCC2 is deviates from the conventional {111} < 112 > system, sharing instead a (402) common plane, as evidenced by Figure 3. At UHSR, abnormal twin growth phenomena are often reported [18,43] and is attributed to the presence of complex triaxial stress states and shock-propagation fields [44]. Moreover, when the entire FCC region is in full contact with the two different CTW variants (Figure 5(d)), twinning occurs throughout the entire FCC domain. This complete twinning leads to well-defined crystallographic relationships with the surrounding CTWs: the twinned FCC maintains a B-type OR with CTW1, while exhibiting a P-type OR with CTW2. Dislocation accumulation

at CTW2 interfaces generate back stress that further promotes CTW2 propagation, ultimately encapsulating the original FCC between CTW1 and CTW2 [39]. Further research efforts well be paid to elucidate the sequence by in-situ TEM and MD simulations.

4. Conclusions

In this study, UHSR deformation-induced HCP-to-FCC transformation and its interactions with deformation twinning were investigated by LSP processing and mutiscale characterization. The experimental results demonstrate the both B- and P-type FCC_{Ti} lamellae are profusely generated and exhibit significant growth capability and intensive interaction with the CTWs. Particularly, two adjacent FCC_{Ti} lamellae with a twinning relationship can be formed within the CTW and matrix, respectively. Moreover, two adjacent FCC_{Ti} lamellae with nearly identical orientation can be formed within the two different CTW variants. These unusual phenomena are elucidated through two proposed scenarios: (i) Phase transformation subsequent to twinning, where FCC lamellae can traverse TBs and CTW-CTW interfaces, facilitated by dislocation transmission or a transition to shear and atomic shuffling; and (ii) Phase transformation accompanied by or prior to twinning, where initial FCC formation is followed by twin impingement, inducing twinning within the FCC regions and enabling twin propagation across FCC domains under intense local stresses.

Disclosure statement

No potential conflict of interest was reported by the author(s).

Funding

Bo Mao acknowledges the funding supports from the National Key R&D Plan of China [grant number 2022YFB3705603], the Excellent Youth Overseas Project of National Science and Natural Foundation of China, the National Natural Science Foundation of China [grant number 52571089], and the Advanced Materials-National Science and Technology Major Project of China [grant number 2025ZD0612000].

References

[1] Ma Y, Chen Y, Yu X, et al. In situ TEM observation of HCP to FCC transitions in hexagonal close-packed titanium. Mater Res Lett. 2024;12(12):956–962. Doi:10.1080/21663831.2024.2404158.

[2] Hong DH, Lee TW, Lim SH, et al. Stress-induced hexagonal close-packed to face-centered cubic phase transformation in commercial-purity titanium under cryogenic plane-strain compression. Scripta Mater. 2013;69(5):405–408. Doi:10.1016/j.scriptamat.2013.05.038.

[3] Wei B, Ni S, Liu Y, et al. Three dimensional crystallographic orientation relationships for hexagonal close packed structure to face centered cubic structure transformation in pure titanium. Scripta Mater. 2019;169:46–51. Doi:10.1016/j.scriptamat.2019.05.010.

[4] Wu HC, Kumar A, Wang J, et al. Rolling-induced face centered cubic titanium in hexagonal close packed titanium at room temperature. Scientific Rep. 2016;6(1):24370. Doi:10.1038/srep24370.

[5] Li Y, Ni S, Liu Y, et al. Phase transition induced high strength and large ductility of a hot rolled near β Ti-5Al-5Mo-5V-1Cr-1Fe alloy. Scripta Mater. 2019;170:34–37. doi:10.1016/j.scriptamat.2019.05.031

[6] Zhu W, Kou W, Tan C, et al. Face centered cubic substructure and improved tensile property in a novel β titanium alloy Ti–5Al–4Zr–10Mo–3Cr. Mater Sci Eng: A. 2020;771:138611. doi:10.1016/j.msea.2019.138611

[7] Yang JX, Zhao HL, Gong HR, et al. Proposed mechanism of HCP→ FCC phase transition in titianium through first principles calculation and experiments. Sci Rep. 2018;8(1):1992. doi:10.1038/s41598-018-20257-9

[8] Zhang H, Wei B, Ou X, et al. Atomic-scale understanding of the reversible HCP↔ FCC phase transition mechanisms at {101¯ 1} twin tip in pure titanium. Int J Plast. 2022;156:103357. doi:10.1016/j.ijplas.2022.103357

[9] Wang S, Niu L, Chen C, et al. Size effects on the tensile properties and deformation mechanism of commercial pure titanium foils. Mater Sci Eng: A. 2018;730:244–261. doi:10.1016/j.msea.2018.06.009

[10] Bai F, Yin L, Zhao W, et al. Deformational behavior of face-centered cubic (FCC) phase in high-pure titanium. Mater Sci Eng: A. 2021;800:140287. doi:10.1016/j.msea.2020.140287

[11] Zheng X, Gong M, Xiong T, et al. Deformation induced FCC lamellae and their interaction in commercial pure Ti. Scripta Materialia. 2019;162:326–330. Doi:10.1016/j.scriptamat.2018.11.037.

[12] Yang C, Li M, Liu Y. Characterization of face-centered cubic structure and deformation mechanisms in high energy shot peening process of TC17. J Mater Sci Technol. 2022;110:136–151. doi:10.1016/j.jmst.2021.08.059

[13] Shahmir H, Langdon TG. An evaluation of the hexagonal close-packed to face-centered cubic phase transformation in a Ti-6Al-4 V alloy during high-pressure torsion. Mater Sci Eng: A. 2017;704:212–217. doi:10.1016/j.msea.2017.07.099

[14] Ma X, Li J, Chen Z, et al. Abnormal work hardening in a TRIP-assisted metastable β titanium alloy under high strain rate loading. Mater Sci Eng: A. 2022;838:142813. doi:10.1016/j.msea.2022.142813

[15] Guan X, Chen Q, Qu S, et al. High-strain-rate deformation: stress-induced phase transformation and nanostructures in a titanium alloy. Int J Plast. 2023;169:103707. doi:10.1016/j.ijplas.2023.103707

[16] Markovsky P, Bondarchuk V. Influence of strain rate, microstructure and chemical and phase composition on mechanical behavior of different titanium alloys. J Mater Eng Perform. 2017;26:3431–3449. doi:10.1007/s11665-017-2781-9

[17] Homayounfard M, Ganjiani M. A large deformation constitutive model for plastic strain-induced phase transformation of stainless steels at cryogenic temperatures. Int J Plast. 2022;156:103344. doi:10.1016/j.ijplas.2022.103344

[18] Mao B, Liao Y, Li B. Abnormal twin-twin interaction in an Mg-3Al-1Zn magnesium alloy processed by laser shock peening. Scripta Materialia. 2019;165:89–93. Doi:10.1016/j.scriptamat.2019.02.028.
[19] Liu Q, Chu S, Zhang X, et al. Laser shock processing of titanium alloys: A critical review on the microstructure evolution and enhanced engineering performance. J Mater Sci Technol. 2025;209:262–291. Doi:10.1016/j.jmst.2024.04.075.
[20] Liu Q, Sun W, Chu S, et al. Quasi-in-situ EBSD study of the thermal stability of gradient twinning microstructure of an AZ31B magnesium alloy processed by laser shock peening. Materials Characterization. 2025;221:114769. Doi:10.1016/j.matchar.2025.114769.
[21] Peyre P, Fabbro R. Laser shock processing: a review of the physics and applications. Optical and Quantum Electronics. 1995;27(12):1213–1229. doi:10.1007/BF00326477
[22] Mao B, Siddaiah A, Menezes PL, et al. Surface texturing by indirect laser shock surface patterning for manipulated friction coefficient. Journal of Materials Processing Technology. 2018;257:227–233. Doi:10.1016/j.jmatprotec.2018.02.041.
[23] Li L, Jia W, Ji V. Effect of laser shock peening on $\alpha \rightarrow \omega$ phase transformation in high-purity titanium. Vacuum. 2022;206:1115. Doi:10.10.1016/j.vacuum.2022.111510.
[24] Xiong L, Zhang S, Zhao C, et al. Revealing in-situ phase transition during laser additive manufacturing via high-speed synchrotron X-ray diffraction and imaging. Mater Res Lett. 2024;12(12):939–946. Doi:10.1080/21663831.2024.2404539.
[25] Yang W, Qian L, Luo J, et al. A novel atomic mechanism of fcc → hcp → bcc phase transition in a gradient nanostructured compositionally complex alloy. Mater Res Lett. 2024;12(12):929–938. Doi:10.1080/21663831.2024.2405228.
[26] Wang B, Liu H, Zhang Y, et al. Effect of grain size on twinning behavior of pure titanium at room temperature. Mater Sci Eng: A. 2021;827:142060. doi:10.1016/j.msea.2021.142060
[27] Chang Y, Zhang S, Liebscher CH, et al. Could face-centered cubic titanium in cold-rolled commercially-pure titanium only be a Ti-hydride? Scripta Mater. 2020;178:39–43. Doi:10.1016/j.scriptamat.2019.11.010.
[28] Traylor R, Zhang R, Kacher J, et al. Impurity and texture driven HCP-to-FCC transformations in Ti-X thin films during in situ TEM annealing and FIB milling. Acta Mater. 2020;184:199–192. Doi:10.10.1016/j.actamat.2019.11.047.
[29] Xie KY, Hazeli K, Dixit N, et al. Twin boundary migration mechanisms in quasi-statically compressed and plate-impacted Mg single crystals. Science Advances. 2021;7(42):eabg3443. doi:10.1126/sciadv.abg3443
[30] Li X, Li J, Zhou B, et al. Interaction of {112¯2} twin variants in hexagonal close-packed titanium. J Mater Sci Technol. 2019;35(4):660–666. Doi:10.1016/j.jmst.2018.09.049.
[31] Wei B, Ni S, Liu Y, et al. Structural characterization of the 112¯2 twin boundary and the corresponding stress accommodation mechanisms in pure titanium. J Mater Sci Technol. 2021;72:114–121. Doi:10.1016/j.jmst.2020.07.030.
[32] Li J, Li X, Yu M, et al. Nucleation mechanism of {101¯2} twin with low schmid factor in hexagonal close-packed metals. Mater Sci Eng: A. 2020;791:139542. Doi:10.1016/j.msea.2020.139542.
[33] Li B, Zhang XY. Global strain generated by shuffling-dominated {101¯2} < 101¯1¯ > twinning. Scripta Mater. 2014;71:45–48. Doi:10.1016/j.scriptamat.2013.10.002.
[34] Wei B, Ni S, Liu Y, et al. Phase transformation and structural evolution in a Ti-5at.% Al alloy induced by cold-rolling. J Mater Sci Technol. 2020;49:211–223. Doi:10.1016/j.jmst.2020.02.032.
[35] Yuan F, Han F, Zhang Y, et al. Intermediate state of hexagonal close-packed structure to face-centered cubic structure transformation: direct evidence for basal-type face-centered cubic phase via partial dislocation in zirconium. J Mater Sci Technol. 2022;98:44–50. Doi:10.1016/j.jmst.2021.05.007.
[36] Hu J, Han F, Ali M, et al. Atomic scale investigation of the phase transformation path from HCP to FCC in high-purity hafnium during torsion deformation. Scripta Mater. 2024;253:116314. Doi:10.1016/j.scriptamat.2024.116314.
[37] Zhao H, Song M, Ni S, et al. Atomic-scale understanding of stress-induced phase transformation in cold-rolled Hf. Acta Mater. 2017;131:271–279. Doi:10.1016/j.actamat.2017.03.058.
[38] Xu S, Wang J. Deformation twins stimulated by {112¯2} twinning in adjacent grain in titanium. Acta Mater. 2022;229:117805. Doi:10.1016/j.actamat.2022.117805.
[39] Arul Kumar M, Capolungo L, McCabe RJ, et al. Characterizing the role of adjoining twins at grain boundaries in hexagonal close packed materials. Sci Rep. 2019;9(1):3846. Doi:10.1038/s41598-019-40615-5.
[40] Kacher J, Robertson IM. In situand tomographic analysis of dislocation/grain boundary interactions in α-titanium. Philos Mag. 2014;94(8):814–829. Doi:10.1080/14786435.2013.868942.
[41] Li J, Sui M, Li B. A half-shear-half-shuffle mechanism and the single-layer twinning dislocation for {112¯2}⟨112¯3¯⟩ mode in hexagonal close-packed titanium. Acta Mater. 2021;216:117150. Doi:10.1016/j.actamat.2021.117150.
[42] Chen P, Wang F, Li B. Misfit strain induced phase transformation at a basal/prismatic twin boundary in deformation of magnesium. Comput Mater Sci. 2019;164:186–194. Doi:10.1016/j.commatsci.2019.04.020.
[43] Zhao F, Wang L, Fan D, et al. Macrodeformation twins in single-crystal aluminum. Phys Rev Lett. 2016 Feb 19;116(7):075501. Doi:10.1103/PhysRevLett.116.075501.
[44] Ding K, Ye L. Laser shock peening. 2006.